Letter

Ultrahigh efficiency plasmonic mode conversion between symmetric and antisymmetric modes in metal slab waveguides by introducing a gyration-managed waveguide link

Kum-Song Ho, Ji-Song Pyon, Jin-Song Kim, Song-Jin Im ◉,* Kum-Dong Kim, Kil-Song Song, Ji-Song Pae, and Chol-Song Ri

*Department of Physics, Kim Il Sung University, Taesong District, 02-381-4410 Pyongyang,
Democratic People's Republic of Korea*

Plasmonic mode conversion is an important topic for realizing the coupling between conventional optical and plasmonic waveguides, and between plasmonic waveguides. However, the switchable mode conversion between the symmetric and the antisymmetric modes propagating along metal slab waveguides, which are among well-known prototypes of surface plasmon polariton (SPP) modes, has never been reported, to our knowledge. In this paper, we suggested the conversion between the symmetric and the antisymmetric modes by introducing a gyration-managed metal slab waveguide link with the zero-averaged gyration. The symmetric (antisymmetric) mode can be converted to the antisymmetric (symmetric) mode with ultrahigh conversion efficiency more than 98%.

DOI: 10.1103/PhysRevB.109.L041402

Thanks to the intrinsic properties of surface plasmon polaritons, which confine light in nanoscale, plasmonic waveguides are regarded as nano-optical waveguides, which are key elements for the development of next-generation integrated nanophotonic circuits [1–3]. Especially, the metal slab, also called the insulator-metal-insulator (IMI) waveguides are considered as one of the most simple and ideal plasmonic nanowaveguides, in which two modes are existed: symmetric and antisymmetric mode, which are so-called long-range (LR) and short-range (SR) SPP modes [3–5]. LRSPPs have a wide range of applications, including biosensors and optical integrated circuits, due to its long propagation length and low loss. And SRSPP has been applied in wideband absorption amplification due to its high mode confinement and loss. Thus, vast research for excitation and control of the plasmon mode in the metal slab waveguides has been performed. Among these, the plasmonic mode converter [6–21] can further enhance the practicability of plasmonics by realizing the coupling between conventional optical mode and plasmonic mode [6–12], and between plasmonic modes [13–21]. However, up to now, the structure for the conversion between plasmonic modes are mainly focused on the metal-insulator-metal (MIM) waveguides [15–19] or metal double wire system [20,21], and most of the mode conversions are achieved by varying path geometry or dielectric environment and by using selective cavities or a actively induced-permittivity asymmetry [13–21]. And the mode conversion between the symmetric and antisymmetric modes in the metal slab waveguide has never been performed, except for a mode conversion between LR and SR modes using a lattice structure in asymmetric dielectric plasmonic waveguide, with a conversion efficiency of up to 18% without switching capabilities in Ref. [14].

On the other hand, the magneto-optical (MO) effect has the advantage of much higher switching speed compared to other effects such as electro-optical [22,23], thermo-optical [24,25] effects. Using magneto-optical effect, the switching speed can be easily reached to the GHz range and modulations in the THz range could also be achieved by controlling the magnetization with femtosecond light pulses [26–30]. This has led to the proposal of magnetoplasmonic modulators [31–38]. In particular, in switchable magnetoplasmonic routers [39,40] the high-contrast plasmonic mode modulation by using the magneto-optical effect in the gyrotropic medium has been suggested, which gives us inspiration to develop useful plasmonic devices such as plasmonic mode converters.

In this paper, we suggested an efficient mode conversion between symmetric and antisymmetric mode based on the MO effect in a metal slab waveguide with gyrotropic medium. In the presence of an external magnetic field, SPP modes in the waveguides exhibit a significant degree of magnetically induced mode asymmetry in its spatial distribution. During the analytical and numerical study, we reveal that the mode asymmetry can be completely reversed by the magnetic field direction inversion and the incident mode switching. On the other hand, it was confirmed that a high-contrast distribution of field intensity to one interface of the waveguide by intermode coupling during propagation through the waveguide and it can also be perfectly switched to the other interface due to the magnetic field direction inversion and the incident mode switching. These interesting results lead us to present a symmetric/antisymmetric mode converter by introducing gyration-inverted waveguide link with a characteristic length and gyration. The proposed system has ultrahigh conversion efficiency more than 98%.

First, we study a mode asymmetry according to magnetic field direction and incident mode. Let us consider plasmon modes propagating in the structure as shown in Fig. 1(a), where a metal film is surrounded by gyrotropic media.

*sj.im@ryongnamsan.edu.kp
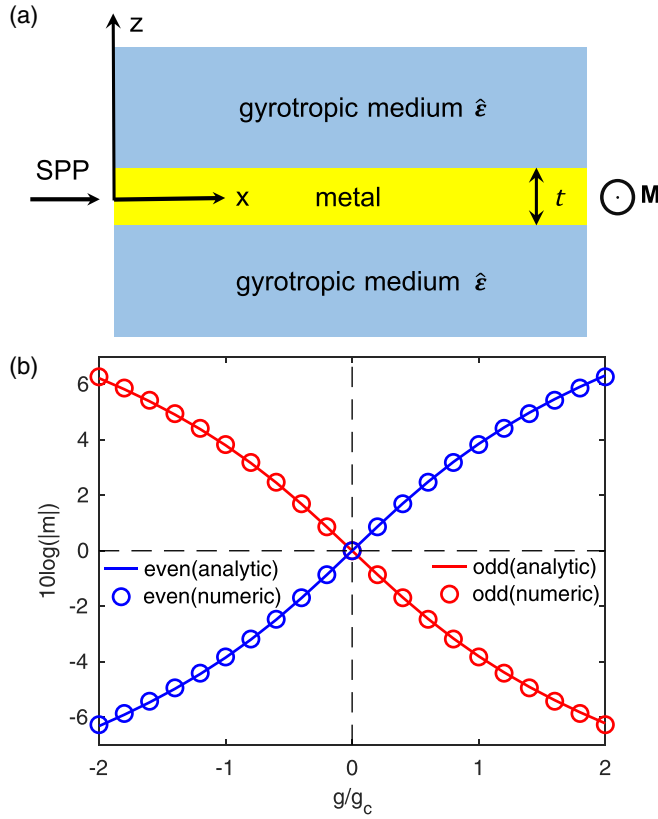
FIG. 1. (a) Metal slab waveguide surrounded by gyrotropic media. The structure is under an external magnetic field M in the transverse y direction. (b) Magnetically induced mode asymmetry of odd and even mode according to g in the magnetoplasmonic waveguide with $t = 100$ nm at $\lambda = 800$ nm, as shown in (a). The solid curves are by Eq. (5) and the circles are by numerical mode solutions of Eq. (2).

The permittivity tensor $\hat{\varepsilon}$ of the gyrotropic medium can be expressed as

$$\hat{\varepsilon} = \begin{pmatrix} \varepsilon_d & 0 & ig \\ 0 & \varepsilon_d & 0 \\ -ig & 0 & \varepsilon_d \end{pmatrix}. \quad (1)$$

Here g is the gyration of the gyrotropic medium under an external magnetic field M in the transverse y direction and is expressed by $g = aM$, where a is the magneto-optical susceptibility. For the fundamental TM mode, we can get the following dispersion relation from the Maxwell equation and boundary conditions:

$$e^{-t/\delta} = \frac{q_m + q_{-g}}{q_m - q_{-g}} \frac{q_m + q_g}{q_m - q_g}, \quad (2)$$

where δ is the Skin depth defined as $\delta = 1/2k_m$, $q_m = k_m/\varepsilon_m$, $q_{-g} = (\varepsilon_d k_d - g\beta)/(\varepsilon_d^2 - g^2)$, $q_g = (\varepsilon_d k_d + g\beta)/(\varepsilon_d^2 - g^2)$, $k_m^2 = \beta^2 - k_0^2 \varepsilon_m$, $k_d^2 = \beta^2 - k_0^2(\varepsilon_2^2 - g^2)/\varepsilon_2$, t is the thickness of the metal film, β is the propagation constant, and ε_m and ε_d are permittivity of the metal and the gyrotropic medium, respectively. From the dispersion relation (2), we can get solutions for two modes: odd and even mode. These modes become the symmetric and antisymmetric modes in the structure in the absence of external magnetic field. However,

an external magnetic field in the transverse y direction induce an asymmetry of the mode distribution. We define degree of the magnetically induced mode asymmetry as

$$m = \left| \frac{H_y(z = -t/2)}{H_y(z = t/2)} \right|, \quad (3)$$

where $H_y(z = -t/2)$ and $H_y(z = t/2)$ are the magnetic field component at the bottom and top interfaces of the waveguide, respectively. From the continuity of the magnetic field component, the asymmetry degree can be expressed as

$$m = \frac{q_m + q_g}{q_m - q_{-g}} e^{t/2\delta}. \quad (4)$$

Let us consider the case that the metal film thickness t is larger than the Skin depth δ. If we assume $g/\varepsilon_d \ll 1$, we can get an analytical expression for the asymmetry as

$$m^{o(e)} \approx (-)\sqrt{1 + (g/g_c)^2} - g/g_c, \quad (5)$$

where the superscripts o and e represent the odd and even modes, respectively. And g_c is a characteristic gyration expressed by

$$g_c = 2\varepsilon_d(-\varepsilon_d/\varepsilon_m)^{1/2} e^{-t/2\delta}. \quad (6)$$

From Eq. (6), the value of g_c is 0.042 if we assume that $t = 100$ nm, $\lambda = 800$ nm, $\varepsilon_d = 6.25$ and the metal is silver. This value can be exponentially reduced by increasing the metal thickness t. In the case of $t = 110$ nm, $g_c = 0.026$, we note that the experimentally observed gyration values of 0.03 or 0.06 for bisubstituted iron garnet (BIG) have been reported [41,42]. As one can see in Eq. (5), for the metal film thickness exceeding the skin depth, the asymmetry degree can be broadly tunable by introducing a small value of g. We note that $g = \pm g_c$ corresponds to $m^o = \sqrt{2} \mp 1$. From Eq. (5), the following valuable relations are easily derived:

$$m(g) \cdot m(-g) = 1,$$
$$m^o \cdot m^e \approx -1. \quad (7)$$

The above relation shows the reversal of magnetically induced mode asymmetry by magnetic field direction inversion and mode switching. We can confirm this relation in Fig. 1(b). This shows the mode asymmetry for the odd (red curves) and even (blue curves) modes with respect to g in the structure of Fig. 1(a), with $t = 100$ nm at $\lambda = 800$ nm. The diagonal permittivity of the gyrotropic medium is assumed to be $\varepsilon_d = 6.25$. The experimental data for the permittivity of silver [43] are used as ε_m. The asymmetry from Eq. (5) (solid curves) agrees well with the results from numerical mode solution of Eq. (2) (circles). In particular, this figure clearly shows the relation (7).

Next, based on above-mentioned mode asymmetry, we study a plasmonic modulation of propagation mode in the metal slab waveguide with two domains under different magnetic field, as shown in Fig. 2(a). Let us assume that the symmetric (antisymmetric) SPP mode is incident to the left port of the structure. At a boundary between the two domains, the incident mode is expanded to a linear combination of odd and even modes,

$$H_y(x, z) = c_1 H_y^o(z) \exp(i\beta^o x) + c_2 H_y^e(z) \exp(i\beta^e x). \quad (8)$$
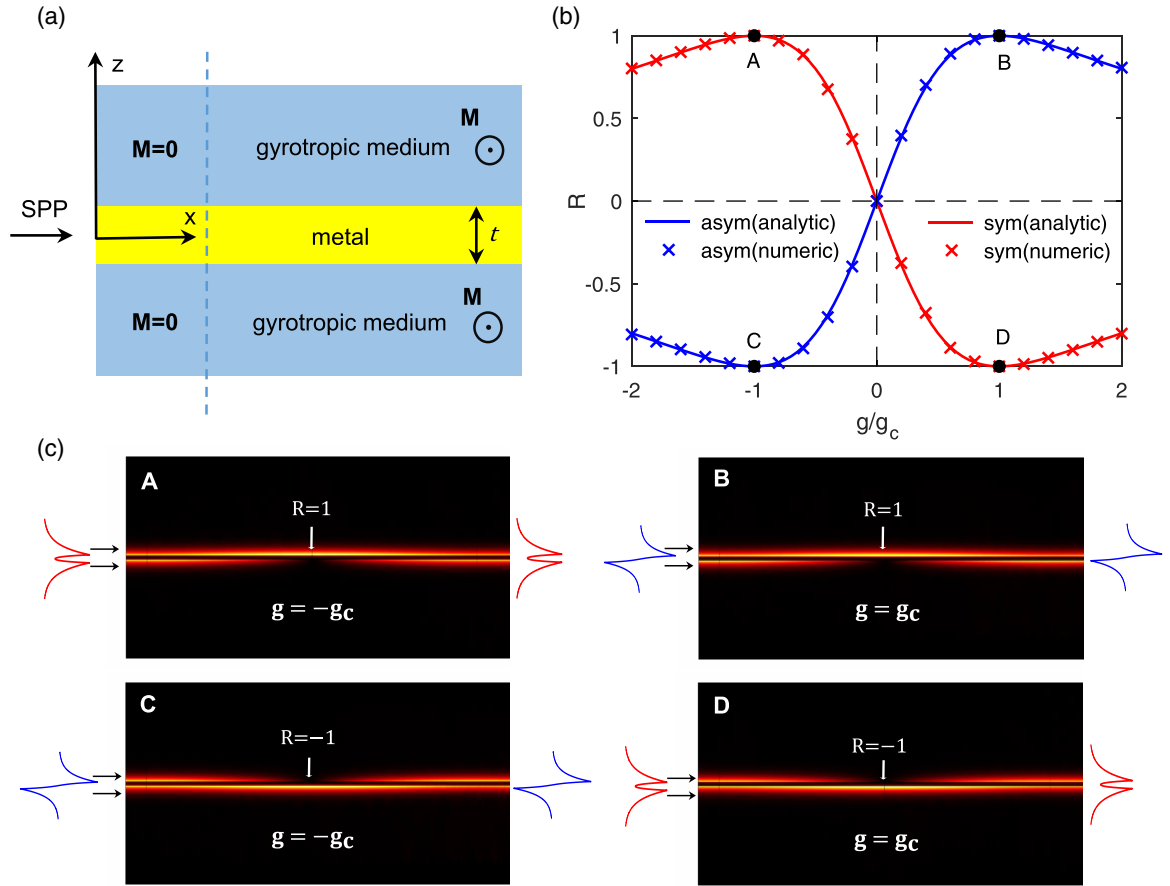
FIG. 2. (a) Configuration for high-contrast plasmonic modulation. It consists of two domains with and without the external magnetic field. (b) The field intensity contrast R between the interfaces of the waveguide of (a) according to g. The red and blue color represent the symmetric and antisymmetric incident mode, respectively. The solid line shows the analytical results by Eq. (12) and the crosses are the numerical results. (c) Numerical simulation results of distribution of $|H_y|^2$ for the points A, B, C, D in (b). Here, the value of g_c (= 0.042) is calculated by Eq. (6). Other parameters are same as in Fig. 1(b). We did not consider the waveguide loss for intuition.

From the continuity of field distribution at the boundary between two domains and Eq. (3), one can obtain the following relation for the expansion coefficients:

$$\frac{c_2}{c_1} \approx \frac{(m^o - p)m^o}{pm^o + 1} \exp\left[\frac{(k_d^e - k_d^o)t}{2}\right]. \quad (9)$$

Here, $p = 1$ for symmetric incident mode and $p = -1$ for antisymmetric mode. While the SPP propagates along the waveguide, the field distribution in the z direction varies due to difference in propagation constant between the odd and even modes $\Delta\beta = \beta^e - \beta^o$. If we remind the assumption $t/\delta \gg 1$ and $g/\varepsilon_d \ll 1$, $\Delta\beta$ is approximately expressed as [39]

$$\Delta\beta \approx \frac{2\beta_0}{1 - \varepsilon_d^2/\varepsilon_m^2} \frac{1}{(-\varepsilon_m - \varepsilon_d)^{1/2}} \sqrt{g_c^2 + g^2}, \quad (10)$$

where the first term is due to difference in wavenumber between the odd and the even modes in the absence of the external magnetic field and the second term is due to the magnetic field. Here, we note that the first term equals to the second term when $g = \pm g_c$.

Now, we define a field intensity contrast between interfaces of the waveguide as

$$R = \left(\frac{\left|H_y\left(x, z = \frac{t}{2}\right)\right|^2 - \left|H_y\left(x, z = -\frac{t}{2}\right)\right|^2}{\left|H_y\left(x, z = \frac{t}{2}\right)\right|^2 + \left|H_y\left(x, z = -\frac{t}{2}\right)\right|^2}\right)_{\text{max}}. \quad (11)$$
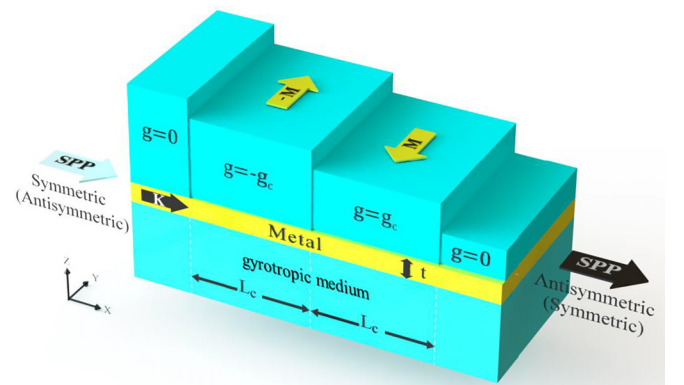
FIG. 3. Scheme of magnetoplasmonic mode converter.
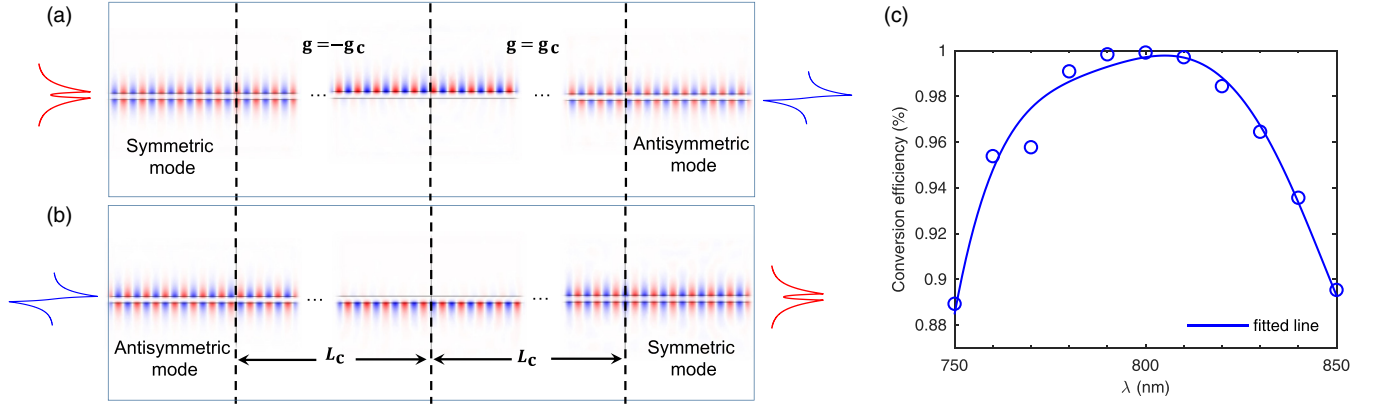
FIG. 4. The process of magnetoplasmonic mode conversion. (a) Symmetric/antisymmetric mode conversion. (b) Antisymmetric/ symmetric mode conversion. (c) The conversion efficiency of the plasmonic mode converter. The solid line is a fitted curve of the numerical results(circle). Here $g_c = 0.042$ and $L_c = 16$ μm have been calculated by Eqs. (6) and (14). Other parameters are the same as in Fig. 1(b). We did not consider the waveguide loss for intuition.

At a propagation length $L = \pi / Re \Delta\beta$, the contrast R is obtained as a following simplified form by using Eqs. (4), (5), and (8)–(11),

$$R^{(s)a} = (-)\frac{2g/g_c}{1 + (g/g_c)^2}, \qquad (12)$$

where the superscript s and a represent symmetric and antisymmetric incident mode, respectively. In Eq. (12), when $g = \pm g_c$, the contrast R becomes its extreme value ± 1 and the high contrast is reversed by switching the magnetic field direction and the incident mode type: symmetric or antisymmetric. Here, $R = 1$ means that the field is concentrated to the upper interface of the waveguide whereas $R = -1$ means that the field is concentrated to the under interface of the waveguide. Equation (12) implies another important relation, which shows the reversal of high-contrast field distribution by magnetic field direction inversion and mode switching,

$$R(g) = -R(-g),$$
$$R^a = -R^s. \qquad (13)$$

Figures 2(b) and 2(c) show the reversal relation of the contrast R in the magnetoplasmonic waveguide, as shown in Fig. 2(a). In Fig. 2(b), we can see the analytical and numerical results of the contrast R according to the gyration g. The red and blue color represent the symmetric and antisymmetric incident mode, respectively. The analytical results are calculated by Eq. (12) and the value of g_c (=0.042) is calculated by Eq. (6). Figure 2(c) shows the numerical simulation results of $|H_y|^2$ distribution for the points A-D in b). Here, one should pay attention to the fact that, despite the different incident mode, the field distribution of A and B, C and D are very similar. If we inverse the gyration at the high-contrast point ($R = 1$) in panel A of which incident mode is symmetric, the output mode will be antisymmetric as in panel B. This is the principle to achieve a mode conversion.

At the value of g_c, using Eq. (10), a characteristic propagation length L_c for the high contrast are obtained by

$$L_c \approx \frac{\pi}{4\sqrt{2}k_0}\left(\frac{\varepsilon_m\varepsilon_d}{\varepsilon_m + \varepsilon_d}\right)^{-1/2}\left(1 - \frac{\varepsilon_d^2}{\varepsilon_m^2}\right)\left(\frac{-\varepsilon_m}{\varepsilon_d}\right)e^{t/2\delta}. \quad (14)$$

In contrast to g_c, L_c exponentially increases with the increase of the metal film thickness t. If the propagation length increases, it causes larger waveguide loss. Thus, an appropriate value of thickness should be selected.

Based on the above results, we suggested a magnetoplasmonic mode converter. The configuration is shown in Fig. 3. It has a gyration-managed waveguide link. Each linking waveguide has a length of L_c and a gyration of $-g_c$ or g_c. As a result, the net gyration in the system is zero. Input SPP mode is incident to the left port of the converter, and the converted mode is output to the right port. Figure 4 shows the conversion process of the mode converter. As can be seen in Figs. 4(a) and 4(b), the incident symmetric mode is perfectly converted to the antisymmetric output mode, and vice versa. In Fig. 4(c), we estimated the efficiency of the suggested converter. As can be seen, the converting efficiency is more than 98% from 780 nm to 820 nm, and more than 90% in a wide band from 750 nm to 850 nm. These results guarantee the ultrahigh efficiency and broadband characteristics of the converter. Here, the conversion efficiency is calculated as a percentage of the targeted mode in the intensity of the output field. And we assumed that $g_c = 0.042$ and $L_c = 16$ μm calculated by Eqs. (6) and (14). While for the sake of physics discussion we did not consider the waveguide loss. We have performed numerical simulations taking into account the absorption in the metal and the BIG (not shown in figures) using the experimental data for the permittivity of silver [43] and the optical loss parameter (the absorption coefficient), 300 dB/cm, for the BIG [44] showing an insertion loss of about 10 dB (a transmission of 10%) for the case of 32 μm length as for Fig. 4(a) and the lower insertion losses for the shorter length. Here, the influence of the absorption in the BIG is quite smaller than that of the absorption in the metal. We note that the absorption in the metal and the BIG does not induce noticeable deterioration to the conversion performance (the conversion efficiency) keeping the 98% efficiency.

In conclusion, we studied analytically and numerically a magnetically induced mode asymmetry and a plasmonic mode conversion in the metal slab waveguide with gyration-managed waveguide link with zero net gyration.

Based on the study, we proposed a symmetric/antisymmetric and antisymmetric/symmetric mode converter with ultrahigh conversion efficiency of more than 98%. The suggested device has a simple structure based on the metal slab waveguide and the high-speed switching capability by using the MO effect. Such a mode converter can be of great importance in the design of high-integration nanophotonic circuits.

---

[1] E. Ozbay, Plasmonics: Merging photonics and electronics at nanoscale dimensions, Science **311**, 189 (2006).

[2] S. I. Bozhevolnyi, V. S. Volkov, E. Devaux, J. Y. Laluet, and T. W. Ebbesen, Channel plasmon subwavelength waveguide components including interferometers and ring resonators, Nature (London) **440**, 508 (2006).

[3] S. Maier, *Plasmonics: Fundamentals and Applications* (Springer, New York, 2007).

[4] P. Berini, Long-range surface plasmon polaritons, Adv. Opt. Photonics **1**, 484 (2009).

[5] Z. Han and S. I. Bozhevolnyi, Radiation guiding with surface plasmon polaritons, Rep. Prog. Phys. **76**, 016402 (2013).

[6] G. Veronis, Z. Yu, S. E. Kocabaş, D. A. B. Miller, M. L. Brongersma, and S. Fan, Metal-dielectric-metal plasmonic waveguide devices for manipulating light at the nanoscale, Chinese Opt. Lett. **7**, 302 (2009).

[7] F. Liu, R. Wan, Y. Li, Y. Huang, Y. Miura, D. Ohnishi, and J. Peng, Extremely high efficient coupling between long range surface plasmon polariton and dielectric waveguide mode, Appl. Phys. Lett. **95**, 091104 (2009).

[8] Y. Ishizaka, M. Nagai, T. Fujisawa, and K. Saitoh, A photonic-plasmonic mode converter using mode-coupling-based polarization rotation for metal-inserted silicon platform, IEICE Electron. Expr. **14**, 20160989 (2017).

[9] A. Melikyan, M. Kohl, M. Sommer, C. Koos, W. Freude, and J. Leuthold, Photonic-to-plasmonic mode converter, Opt. Lett. **39**, 3488 (2014).

[10] Y. T. Hung, C. B. Huang, and J. S. Huang, Plasmonic mode converter for controlling optical impedance and nanoscale light-matter interaction, Opt. Express **20**, 20342 (2012).

[11] M. Ono, H. Taniyama, E. Kuramochi, K. Nozaki, and M. Notomi, Toward application of plasmonic waveguides to optical devices, NTT Tech. Rev. **16**, 14 (2018).

[12] M. Ono, H. Taniyama, H. Xu, M. Tsunekawa, E. Kuramochi, K. Nozaki, and M. Notomi, Deep-subwavelength plasmonic mode converter with large size reduction for Si-wire waveguide, Optica **3**, 999 (2016).

[13] D. Pan, H. Wei, Z. Jia, and H. Xu, Mode conversion of propagating surface plasmons in nanophotonic networks induced by structural symmetry breaking, Sci. Rep. **4**, 4993 (2014).

[14] H. Zhang, Y. Li, N. Zhu, G. Jin, D. Zhang, and T. Mei, Mode conversion in asymmetric dielectric/metal/dielectric plasmonic waveguide using grating coupler, Opt. Commun. **310**, 217 (2014).

[15] R. H. Kabeel, N. F. F. Areed, M. F. O. Hameed, and S. S. A. Obayya, Efficient tunable plasmonic mode converters infiltrated with nematic liquid crystal layers, Opt. Quantum Electron. **53**, 436 (2021).

[16] Y. Wang and X. Yan, Mode conversion in metal-insulator-metal waveguide with a shifted cavity, Jpn. J. Appl. Phys. **57**, 010303 (2018).

[17] X. T. Kong, Z. B. Li, and J. G. Tian, Mode converter in metal-insulator-metal plasmonic waveguide designed by transformation optics, Opt. Express **21**, 9437 (2013).

[18] M. Khatir and N. Granpayeh, A wide band and high confinement surface plasmon polariton mode converter based on magneto-optic effects, IEEE Trans. Magn. **49**, 1343 (2013).

[19] B. Liu, Y.-F. Liu, S.-J. Li, and X.-D. He, Rotation and conversion of transmission mode based on a rotatable elliptical core ring resonator, Opt. Commun. **369**, 44 (2016).

[20] W.-H. Dai, F.-C. Lin, C.-B. Huang, and J.-S. Huang, Mode conversion in high-definition plasmonic optical nanocircuits, Nano Lett. **14**, 3881 (2014).

[21] S. Sun, H. T. Chen, W. J. Zheng, and G. Y. Guo, Dispersion relation, propagation length and mode conversion of surface plasmon polaritons in silver double-nanowire system, Opt. Express **21**, 14591 (2013).

[22] J. S. Schildkraut, Long-range surface plasmon electro-optic modulator, Appl. Opt. **27**, 4587 (1988).

[23] A. Melikyan, L. Alloatti, A. Muslija, D. Hillerkuss, P. C. Schindler, J. Li, R. Palmer, D. Korn, S. Muehlbrandt, D. Van Thourhout, B. Chen *et al.*, High-speed plasmonic phase modulators, Nat. Photon. **8**, 229 (2014).

[24] C. Haffner, W. Heni, Y. Fedoryshyn, J. Niegemann, A. Melikyan, D. L. Elder, B. Baeuerle, Y. Salamin, A. Josten, U. Koch *et al.*, All-plasmonic Mach-Zehnder modulator enabling optical high-speed communication at the microscale, Nat. Photon. **9**, 525 (2015).

[25] J. Gosciniak and S. I. Bozhevolnyi, Performance of thermo-optic components based on dielectric-loaded surface plasmon polariton waveguides, Sci. Rep. **3**, 1803 (2013).

[26] G. Armelles, A. Cebollada, A. García-Martín, and M. U. González, Magnetoplasmonics: Combining magnetic and plasmonic functionalities, Adv. Opt. Mater. **1**, 10 (2013).

[27] A. V. Kimel, A. Kirilyuk, P. A. Usachev, R. V. Pisarev, A. M. Balbashov, and T. Rasing, Ultrafast non-thermal control of magnetization by instantaneous photomagnetic pulses, Nature (London) **435**, 655 (2005).

[28] A. Kirilyuk, A. V. Kimel, and T. Rasing, Ultrafast optical manipulation of magnetic order, Rev. Mod. Phys. **82**, 2731 (2010).

[29] S.-J. Im, C.-S. Ri, K.-S. Ho, and J. Herrmann, Third-order nonlinearity by the inverse Faraday effect in planar magneto-plasmonic structures, Phys. Rev. B **96**, 165437 (2017).

[30] S.-J. Im, J.-S. Pae, C.-S. Ri, K.-S. Ho, and J. Herrmann, All-optical magnetization switching by counterpropagataion or two-frequency pulses using the plasmon-induced inverse Faraday effect in magnetoplasmonic structures, Phys. Rev. B **99**, 041401(R) (2019).

[31] V. V. Temnov, G. Armelles, U. Woggon, D. Guzatov, A. Cebollada, A. García-Martín, J. M. García-Martín, T. Thomay, A. Leitenstorfer, and R. Bratschitsch, Active

magneto-plasmonics in hybrid metal-ferromagnet structures, Nat. Photon. **4**, 107 (2010).

[32] V. Belotelov, L. Kreilkamp, I. Akimov, A. Kalish, D. Bykov, S. Kasture, V. Yallapragada, A. V. Gopal, A. Grishin, S. Khartsev *et al.*, Plasmon-mediated magneto-optical transparency, Nat. Commun. **4**, 2128 (2013).

[33] Y. S. Dadoenkova, N. N. Dadoenkova, I. L. Lyubchanskii, J. W. Klos, and M. Krawczyk, Faraday effect in biperiodic photonic-magnonic crystals, IEEE Trans. Magn. **53**, 1 (2017).

[34] J.-S. Pae, S.-J. Im, K.-S. Ho, C.-S. Ri, S.-B. Ro, and J. Herrmann, Ultracompact high-contrast magneto-optical disk resonator side-coupled to a plasmonic waveguide and switchable by an external magnetic field, Phys. Rev. B **98**, 041406(R) (2018).

[35] D. O. Ignatyeva, D. Karki, A. A. Voronov, M. A. Kozhaev, D. M. Krichevsky, A. I. Chernov, and M. Levy, All-dielectric magnetic metasurface for advanced light control in dual polarizations combined with high-Q resonances, Nat. Commun. **11**, 5487 (2020).

[36] Y. R. Fang, Z. P. Li, Y. Z. Huang, S. P. Zhang, P. Nordlander, N. J. Halas, and H. X. Xu, Branched silver nanowires as controllable plasmon routers, Nano Lett. **10**, 1950 (2010).

[37] Z. F. Yu, G. Veronis, Z. Wang, and S. H. Fan, One-way electromagnetic waveguide formed at the interface between a

plasmonic metal under a static magnetic field and a photonic crystal, Phys. Rev. Lett. **100**, 023902 (2008).

[38] J.-M. Pak, J.-S. Pae, S.-J. Im, S.-C. Kim, U.-S. Kim, K.-D. Kim, K.-S. Song, and Y.-H. Han, Gain-assisted magnetoplasmonic switching in metal-dielectric-metal plasmonic waveguides, Appl. Phys. Lett. **123**, 131112 (2023).

[39] K.-S. Ho, S.-J. Im, J.-S. Pae, C.-S. Ri, Y.-H. Han, and J. Herrmann, Switchable plasmonic routers controlled by external magnetic fields by using magneto-plasmonic waveguides, Sci. Rep. **8**, 10584 (2018).

[40] K.-D. Kim, S.-J. Im, K.-S. Song, J.-S. Pae, C.-S. Ri, K.-S. Ho, and Y.-H. Han, Magnetic resonance of plasmonic modulation and switchable routing in gated graphene waveguides and their robustness and broadband tunability, Phys. Rev. B **106**, L041401 (2022).

[41] S. Yao, T. Sato, K. Kaneko, S. Murai, K. Fujita, and K. Tanaka, Faraday effect of bismuth iron garnet thin film prepared by mist CVD method, Jpn. J. Appl. Phys. **54**, 063001 (2015).

[42] A. Dutta, A. V. Kildishev, V. M. Shalaev, A. Boltasseva, and E. E. Marinero, Surface-plasmon opto-magnetic field enhancement for all-optical magnetization switching, Opt. Mater. Express **7**, 4316 (2017).

[43] P. B. Johnson and R. W. Christy, Optical constants of the noble metals, Phys. Rev. B **6**, 4370 (1972).

[44] A. K. Zvezdin and V. A. Kotov, *Modern Magnetooptics and Magnetooptical Materials* (IOP Publishing, Bristol, 1997).